ARTICLE

doi:10.1038/nature09816

Linear ubiquitination prevents inflammation and regulates immune signalling

Björn Gerlach[1,2]*, Stefanie M. Cordier[1]*, Anna C. Schmukle[1]*, Christoph H. Emmerich[1,2]*, Eva Rieser[1]*, Tobias L. Haas[2,3]*, Andrew I. Webb[4]*, James A. Rickard[5], Holly Anderton[5], Wendy W.-L. Wong[5], Ueli Nachbur[5], Lahiru Gangoda[5], Uwe Warnken[6], Anthony W. Purcell[4], John Silke[5] & Henning Walczak[1,2]

Members of the tumour necrosis factor (TNF) receptor superfamily have important functions in immunity and inflammation. Recently linear ubiquitin chains assembled by a complex containing HOIL-1 and HOIP (also known as RBCK1 and RNF31, respectively) were implicated in TNF signalling, yet their relevance *in vivo* remained uncertain. Here we identify SHARPIN as a third component of the linear ubiquitin chain assembly complex, recruited to the CD40 and TNF receptor signalling complexes together with its other constituents, HOIL-1 and HOIP. Mass spectrometry of TNF signalling complexes revealed RIP1 (also known as RIPK1) and NEMO (also known as IKKγ or IKBKG) to be linearly ubiquitinated. Mutation of the *Sharpin* gene (*Sharpin*$^{cpdm/cpdm}$) causes chronic proliferative dermatitis (*cpdm*) characterized by inflammatory skin lesions and defective lymphoid organogenesis. Gene induction by TNF, CD40 ligand and interleukin-1β was attenuated in *cpdm*-derived cells which were rendered sensitive to TNF-induced death. Importantly, *Tnf* gene deficiency prevented skin lesions in *cpdm* mice. We conclude that by enabling linear ubiquitination in the TNF receptor signalling complex, SHARPIN interferes with TNF-induced cell death and, thereby, prevents inflammation. Our results provide evidence for the relevance of linear ubiquitination *in vivo* in preventing inflammation and regulating immune signalling.

Members of the TNF receptor superfamily (TNFRSF) exert pleiotropic effects in immune and non-immune tissues[1] and their signalling is regulated by different types of ubiquitin chains[2–4]. We and others recently showed that pro-survival signalling by TNF receptor 1 (TNFR1) was compromised in cells deficient in HOIL-1 or HOIP and that these cells were sensitized to TNF-induced cell death[5,6]. Together, HOIL-1 and HOIP form the linear ubiquitin chain assembly complex (LUBAC) which catalyses the formation of a peptide bond between the amino-terminal methionine (M1) of one ubiquitin molecule and the carboxy-terminal glycine (G76) of the next. Therefore, linear ubiquitin linkage is also referred to as M1 linkage. LUBAC is recruited to the TNF receptor signalling complex (RSC)[5] and its linear-ubiquitin-chain-generating activity is required in the TNF-RSC for efficient gene activation and prevention of apoptosis induction by TNF[5,6]. This has been suggested to be due to LUBAC-mediated linear ubiquitination of NEMO[6]. NEMO can bind both lysine 63 (K63)-linked and linear ubiquitin chains[7–9]. Therefore we proposed that LUBAC and its linear-ubiquitin-chain-forming activity are important for efficient NEMO recruitment to, and retention in, the TNF-RSC and consequent TNF-induced gene activation[5]. The relevance of LUBAC and linear ubiquitination *in vivo*, however, remains unknown and contested[10].

SHARPIN is recruited to CD40- and TNF-RSCs

We recently reported on the identification of HOIL-1 and HOIP as novel components of the TNF-RSC by tandem-mass-spectrometry following isolation of this protein complex by modified tandem affinity purification (moTAP)[5]. We developed a similar moTAP approach for CD40L (also known as CD154 or CD40LG; Supplementary Fig. 1a–c) and purified the native CD40-RSC (Fig. 1a). This analysis revealed HOIL-1, HOIP as well as SHARPIN as potential novel components of the CD40-RSC (Supplementary Fig. 2a). SHARPIN was also the only other novel protein, apart from HOIL-1 and HOIP[5], for which peptides were identified by mass-spectrometry following moTAP of the TNF-RSC (Supplementary Fig. 2b). Using a SHARPIN-specific monoclonal antibody (Supplementary Fig. 3a) we next showed that SHARPIN was indeed recruited to both, the CD40-RSC and the TNF-RSC in a ligand- and time-dependent manner, with similar kinetics as HOIL-1 and HOIP (Fig. 1b and Supplementary Fig. 3b). We showed previously that recruitment of HOIL-1 and HOIP to the TNF-RSC depended on the presence and E3 activity of cellular inhibitor of apoptosis proteins (cIAPs)[5]. We therefore tested whether SHARPIN recruitment also required cIAPs by using the Smac (also known as DIABLO)-mimetic compound SM-164 (ref. 11). Treatment of cells with SM-164 resulted in rapid and complete depletion of cIAPs over the entire time course of the experiment (Fig. 1c, d). This pre-treatment prevented RIP1 ubiquitination in TNF-treated cells (Fig. 1d) and almost completely abolished recruitment of HOIL-1, HOIP and SHARPIN to both the CD40-RSC (Fig. 1c) and the TNF-RSC (Fig. 1d and ref. 5).

Complexes of SHARPIN, HOIL-1 and HOIP generate linear ubiquitin chains

In addition to the sequence similarity between SHARPIN and HOIL-1 (Supplementary Fig. 3c), these results indicated that SHARPIN may be recruited to the CD40- and TNF-RSCs together with HOIP and/or

[1]Tumour Immunology Unit, Department of Medicine, Imperial College London, W12 0NN London, UK. [2]Division of Apoptosis Regulation, German Cancer Research Center (DKFZ), 69120 Heidelberg, Germany. [3]Department of Experimental Oncology, Mediterranean Institute of Oncology, 95029 Viagrande, Italy. [4]Department of Biochemistry, Bio21 Melbourne University, Melbourne, VIC 3010, Australia. [5]Department of Biochemistry, La Trobe University, Melbourne, VIC 3086, Australia. [6]Protein Analysis Core Facility, German Cancer Research Center (DKFZ), 69120 Heidelberg, Germany.
*These authors contributed equally to this work.

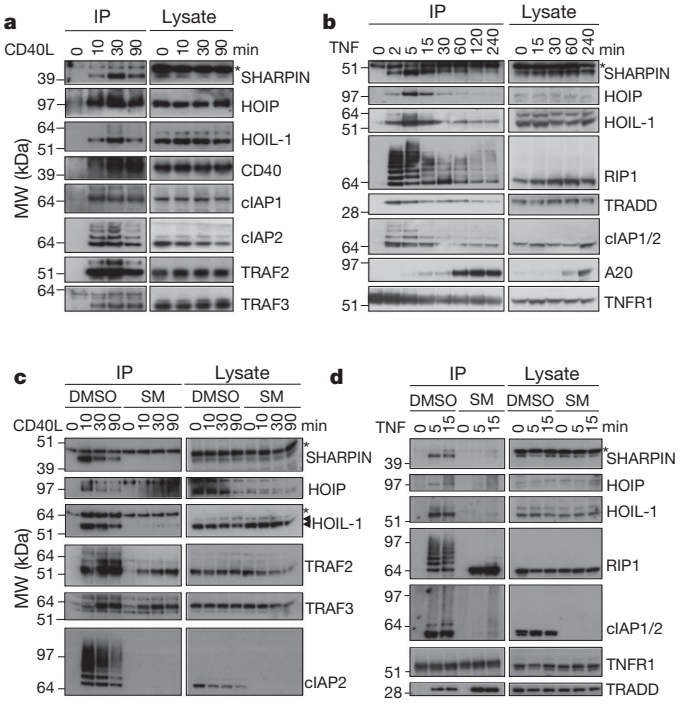

Figure 1 | SHARPIN is recruited to the native CD40- and TNF-RSCs. **a**, **b**, SHARPIN, HOIL-1 and HOIP are recruited to the native CD40- and TNF-RSC in Raji B cells (**a**) and HeLa cells (**b**), respectively. **c**, **d**, Raji (**c**) and HeLa (**d**) cells were pre-treated for 2 h with SM-164 (SM) before the CD40- (**c**) and TNF-RSCs (**d**) were precipitated at the indicated times. IP, immunoprecipitation; *, unspecific bands.

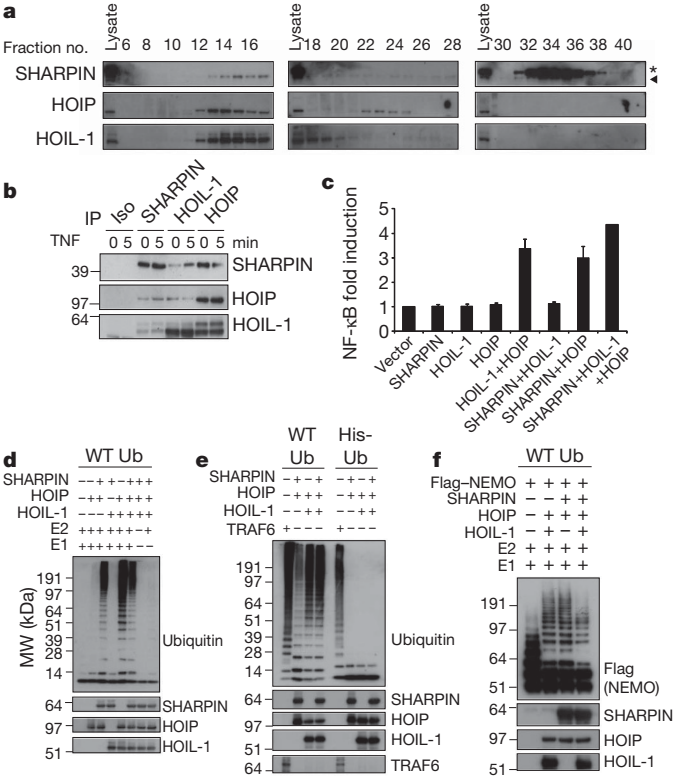

Figure 2 | SHARPIN forms a tripartite complex with HOIP and HOIL-1 that is capable of forming linear ubiquitin chains. **a**, SHARPIN, HOIL-1 and HOIP co-elute in high molecular weight S100 cytosolic fractions in HeLa cells. *, unspecific band. **b**, SHARPIN, HOIL-1 and HOIP form a stimulation-independent complex. Iso, isotype control. **c**, SHARPIN activates NF-κB when co-expressed with HOIP or HOIP and HOIL-1. Proteins were overexpressed in 293-NF-κB cells and a luciferase-reporter assay was performed ($n = 4$). Data are presented as mean ± s.e.m. **d**, **e** SHARPIN contributes to linear ubiquitin chain formation when complexed with HOIP or HOIP and HOIL-1. Ub, ubiquitin; WT, wild type. **f**, HOIP in combination with SHARPIN and/or HOIL-1 attaches ubiquitin chains to NEMO.

HOIL-1 and possibly cooperates with them functionally. To test this hypothesis we examined the possibility of endogenous complex formation between SHARPIN and HOIL-1/HOIP. Gel filtration analysis showed that the three endogenous proteins eluted together in the same high-molecular-weight fractions, with SHARPIN being shifted away from a strongly reactive but unspecific band that remained in the low-molecular-weight fractions (Fig. 2a). In addition, co-immunoprecipitation experiments showed that the endogenous proteins were also bound to each other independently of TNF stimulation (Fig. 2b). These results strongly indicate the existence of a tripartite protein complex consisting of HOIP, SHARPIN and HOIL-1, but do not rule out the existence of additional functionally active complexes consisting of other combinations of these proteins.

We next investigated the functionality of SHARPIN interactions with HOIL-1 and/or HOIP. SHARPIN was unable to activate NF-κB when expressed alone, or when combined with HOIL-1, yet when combined with HOIP, NF-κB was activated to a similar level as when HOIL-1 and HOIP were co-expressed. Overexpression of all three components together resulted in the strongest NF-κB activation (Fig. 2c). This pointed to an essential role for HOIP in the functional activity of the different combinations. Using deletion and point mutants of SHARPIN and HOIP (Supplementary Fig. 4a) we determined that the interaction between these two proteins is primarily due to the ubiquitin-like (UBL) domain of SHARPIN binding to the second Npl4 zinc-finger domain (NZF2) of HOIP (Supplementary Fig. 4b–d and Supplementary Fig. 5a, b). In addition, via its NZF domain SHARPIN binds to ubiquitin (Supplementary Fig. 6a, b), preferring M1- and K63- over K48-linked ubiquitin tetramers (Supplementary Fig. 6c).

Activation of NF-κB by simultaneous overexpression of HOIL-1 and HOIP correlates with their ability to generate linear ubiquitin chains[6]. We therefore tested the ability of recombinant SHARPIN in combination with recombinant HOIL-1 and/or HOIP to generate M1-linked ubiquitin chains. In accord with their respective abilities to activate NF-κB, combinations of SHARPIN–HOIP–HOIL-1, SHARPIN–HOIP and HOIP–HOIL-1, but not of SHARPIN–HOIL-1, were capable of forming ubiquitin chains (Fig. 2d). His-tagged ubiquitin (His-ubiquitin) is blocked at the N terminus and capable of contributing to all ubiquitin chain linkages except for linear ones. Accordingly, TRAF6, a control E3 that forms nonlinear chains, was capable of using both wild-type and His-ubiquitin to generate polyubiquitin chains (Fig. 2e). The three active LUBAC combinations were, however, capable of generating ubiquitin chains only with wild-type but not His-ubiquitin (Fig. 2e). This demonstrates that, in addition to the LUBAC consisting of HOIL-1 and HOIP described previously, a second dimeric LUBAC consisting of SHARPIN and HOIP, as well as a third LUBAC, the tripartite complex consisting of SHARPIN, HOIP and HOIL-1, exclusively generate linear ubiquitin chains.

RIP1 and NEMO are linearly ubiquitinated in the TNF-RSC

To test whether the three different LUBAC versions may share and/or act differentially on various possible targets, we investigated their ability to modify components of the CD40- and TNF-RSCs *in vitro*. This analysis revealed that all three LUBAC versions were capable of ubiquitinating NEMO *in vitro* (Fig. 2f). Yet none of the eight other CD40- and/or TNF-RSC components tested were modified to any significant extent (Supplementary Figs 7 and 8), except RIP1 on which subtle modification was detected. To investigate the *in vivo* relevance of these findings we developed a highly specific and sensitive method to enable the analysis of isolated, individual RSC components

(Supplementary Figs 9 and 10) by combining moTAP with fluorescence protein labelling, two-dimensional (2D) separation, fluorescence-guided robotic spot picking, tryptic digestion and multiple reaction monitoring (MRM) mass spectrometry. This moTAP-2D-MRM approach (Fig. 3) showed that both RIP1 and NEMO are linearly ubiquitinated in the native TNF-RSC (Fig. 3 and Supplementary Figs 11 and 12). In each of two individual RIP1-containing spots, in addition to the signature peptide of linear ubiquitin linkage (Ub-M1), we also identified signature peptides identifying K11-, K48- and K63-linked ubiquitin (Fig. 3a, c, Supplementary Figs 11 and 12 and data not shown for RIP1 spot B). The NEMO spot we analysed, however, contained exclusively M1-linked ubiquitin (Fig. 3b, d and Supplementary Figs 11 and 12). Thus, RIP1 and NEMO reside as linearly ubiquitinated proteins in the native TNF-RSC.

SHARPIN is required for TNF, CD40L and IL-1β signalling

We next assessed whether any one of the three LUBAC components was required for LUBAC recruitment to the TNF-RSC. Suppression of HOIL-1 resulted in only slight reduction of SHARPIN and HOIP in the TNF-RSC (Supplementary Fig. 13a), indicating that HOIL-1 is not required for their recruitment. Suppression of HOIP on the other hand completely abrogated recruitment of HOIL-1 and SHARPIN to the TNF-RSC (Fig. 4a). To test the role of SHARPIN, we took advantage of the chronic proliferative dermatitis (cpdm) strain of BL/6 mice that carry a spontaneous mutation in the *Sharpin* gene[12]. Although murine embryonic fibroblasts (MEFs) generated from *Sharpin*$^{cpdm/cpdm}$ (*cpdm*) mice expressed less HOIL-1 and HOIP than wild-type MEFs (Supplementary Fig. 14a), recruitment of HOIL-1 and HOIP to the TNF-RSC still occurred, albeit at a lower level than in wild-type MEFs (Supplementary Fig. 13b). Importantly, reduced protein levels of HOIL-1 and HOIP in *cpdm* MEFs was not due to decreased mRNA levels for these proteins (Supplementary Fig. 14b), indicating that SHARPIN stabilizes HOIL-1 and HOIP at the protein level. This finding provides further indirect evidence for the existence of a tripartite LUBAC. Taken together, neither HOIL-1 nor SHARPIN are required for LUBAC recruitment to the TNF-RSC, but HOIP as the central component is. Interestingly, the recruitment of SHARPIN

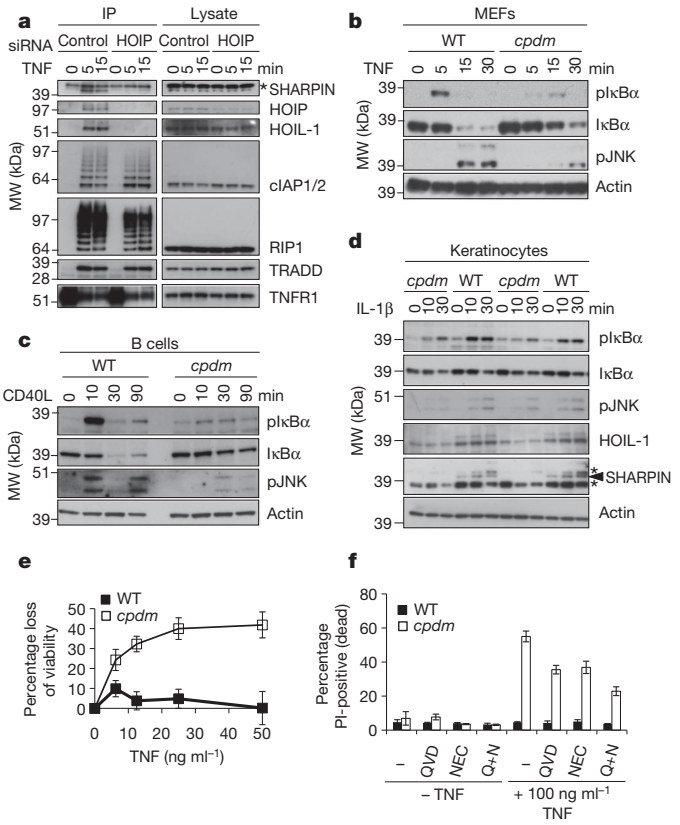

Figure 4 | SHARPIN is required for full TNF-, CD40L- and IL-1β-induced activation of NF-κB and JNK and to prevent TNF-induced cell death. **a**, Recruitment of the HOIP–HOIL-1/SHARPIN complex to the TNF-RSC is mediated by HOIP. **b**–**d**, SHARPIN is required for efficient TNF- (**b**), CD40L- (**c**) and IL-1β-induced (**d**) NF-κB and JNK activation. pIκBα and pJNK, phosphorylated IκBα and JNK. **e**, **f**, Absence of SHARPIN sensitises MEFs to TNF-induced cell death as determined by (**e**) cell viability measurement ($n = 4$) and (**f**) propidium iodide (PI) incorporation ($n = 6$). Data are presented as mean ± s.e.m.

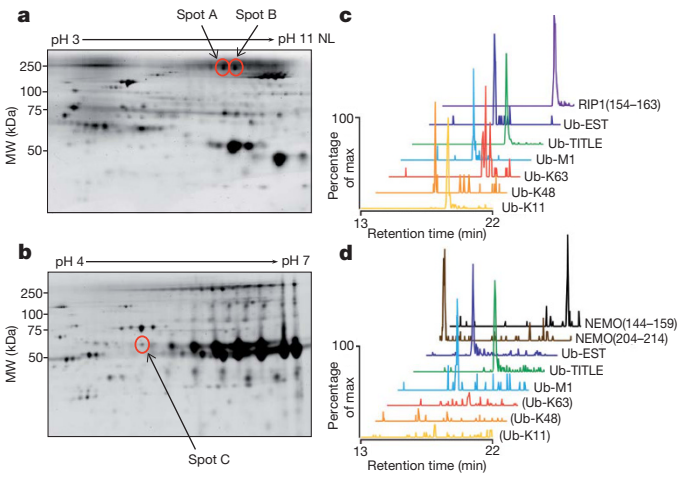

Figure 3 | NEMO and RIP1 are linearly ubiquitinated in the native TNF-RSC. **a**, **b**, Fluorescence images of 2D gels of moTAP-purified CyDye-stained TNF-RSC. U937 cells (3×10^9, **a**; and 1.8×10^{10}, **b**) were stimulated with moTAP-TNF before tandem purification of the TNF-RSC, fluorescence labelling and 2D separation. Red circles indicate spots in which RIP1 and ubiquitin (**a**) and NEMO and ubiquitin (**b**) were detected, respectively. **c**, Extracted ion chromatograms (XICs) for all peptides detected in spot A. Enhanced product ion (EPI) spectra, confirming the MRM transition, were observed for all peptides shown (Supplementary Fig. 7). **d**, XICs for all peptides detected in spot C. EST and TITLE, the ubiquitin-derived tryptic peptides ESTLHLVLR and TITLEVEPSDTIENVK.

and HOIP in HOIL-1-suppressed cells, and of HOIL-1 and HOIP in SHARPIN-deficient cells (Supplementary Fig. 13a, b), shows that at least in the absence of the respective third component, complexes of the other two exist and can be recruited to RSCs.

Mutation of the *Sharpin* gene is causative for the *cpdm* phenotype[12–14]. In addition to the skin, many other tissues including liver, lung, forestomach and oesophagus, are also inflamed in *cpdm* mice[13]. *Cpdm* mice also present with a prominent immunological phenotype characterized by lymphoid dysregulation, splenomegaly, defects in T_H1 cytokine production and various lymphoid developmental and structural abnormalities[13–15].

Therefore, we next examined immune cytokine signalling in cells obtained from *cpdm* mice. We showed previously that suppression of HOIL-1 and HOIP negatively affected activation of the NF-κB and JNK pathways as well as gene induction following TNF stimulation[5]. Consistent with this, we found that *cpdm* MEFs also activated NF-κB poorly in response to TNF. In particular, these cells showed decreased phosphorylation and degradation of IκBα (Fig. 4b), impaired and delayed nuclear translocation of the NF-κB subunit p65 (Supplementary Fig. 15a, b) and reduced induction of TNF target genes when compared to wild-type MEFs (Supplementary Fig. 16a). Intriguingly, induction of IκBα was substantially less affected than that of other target genes (Supplementary Fig. 16a). This might be explained by a recent finding showing that induction of certain NF-κB target genes, for example, IκBα, was relatively independent of signal strength and occurred even at low doses of TNF, whereas that of others required high doses and a strong TNF response[16]. The additional reduction of

JNK activation in TNF-stimulated *cpdm* MEFs (Fig. 4b) indicates that genes which require cooperation between NF-κB and JNK for their expression will be particularly affected by defective LUBAC recruitment or absence of LUBAC components. Our findings in TNF-stimulated *cpdm* MEFs are corroborated by defective CD40L-induced NF-κB and JNK activation in splenic *cpdm* B cells (Fig. 4c and Supplementary Fig. 17a, b). Importantly, in primary keratinocytes obtained from the skin of 2-week-old non-diseased *cpdm* mice (skin being the tissue most strongly affected by loss of SHARPIN) activation of NF-κB and JNK by both IL-1β and TNF was also attenuated (Fig. 4d and Supplementary Fig. 18). By contrast, CD40L- and TWEAK (also known as TNFSF12)-induced processing of p100 to p52 were not significantly altered in *cpdm*-derived B-cells and MEFs, respectively (Supplementary Fig. 17b, c and Supplementary Fig. 19). However, given the similarity in lymphoid organogenesis defects between *cpdm* mice and mice in which non-canonical NF-κB is defective[17], on the basis of these results we do not rule out the possibility that in cells responsible for proper lymphoid organ development non-canonical NF-κB activity might be negatively affected, either directly or indirectly, by the absence of SHARPIN.

Additional suppression of HOIL-1 in *cpdm* MEFs further decreased TNF-induced destabilization and phosphorylation of IκBα compared to *cpdm* MEFs (Supplementary Fig. 15c). However, activation of NF-κB still occurred. This demonstrates that SHARPIN and, consequently, LUBAC activity are not essential for TNF-induced activation of NF-κB but that they are important for regulating the strength of signal transduction and hence gene expression following TNF stimulation.

Given our previous finding that suppression of HOIL-1 or HOIP by RNA interference sensitises cells to TNF-induced death[5], we next tested whether the *cpdm* mutation also had an impact on survival following TNF stimulation. We found that *cpdm* MEFs were highly sensitive to TNF-induced cell death (Fig. 4e, f). This cell death was partially blocked by the apoptosis inhibitor Q-Val-Asp(non-*O*-methylated)-OPh (QVD) and the necroptosis inhibitor necrostatin-1 (NEC) and most efficiently inhibited by a combination thereof (Fig. 4f). Thus, TNF-induced cell death in *cpdm* MEFs includes an apoptotic (Supplementary Fig. 20) as well as a necroptotic component. Taken together, these results demonstrate that loss of SHARPIN results in a gene-induction-inhibitory dysregulation of cytokine signalling and sensitisation to TNF-induced cell death.

Ablation of TNF rescues *cpdm* skin phenotype

Increased rates of keratinocyte cell death have been described in the skin of *cpdm* mice[14,18]. Given that our analysis of TNF signalling pathways in *cpdm* MEFs revealed sensitisation to TNF-induced cell death we reasoned that removal of TNF might alleviate or even prevent inflammation in *cpdm* mice. We therefore crossed *cpdm* mice with TNF-deficient mice. Strikingly, we found that deletion of only one allele of the *Tnf* gene prevented the occurrence of macroscopic and microscopic skin lesions in *cpdm* mice (Fig. 5a, b and Supplementary Fig. 21). In contrast to the rescue of the skin phenotype, many other

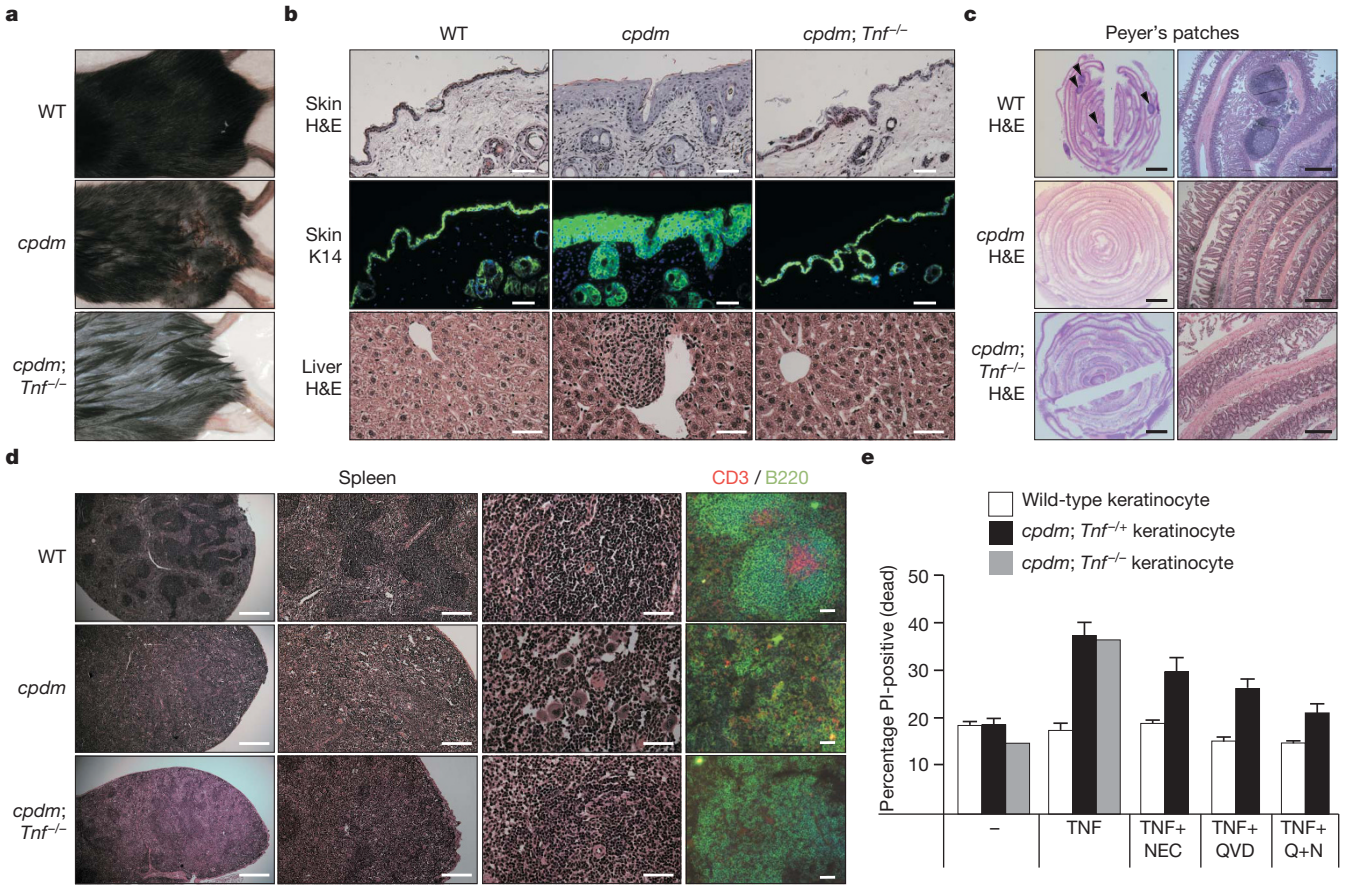

Figure 5 | Genetic ablation of TNF rescues the skin phenotype and reduces inflammation in *cpdm* mice but does not revert the immunological distortion. **a**, Loss of TNF restores normal skin morphology in *cpdm* mice. **b**, Inflammatory skin and liver lesions do not develop in *cpdm*;*Tnf*$^{-/-}$ mice as shown by haematoxylin and eosin (H&E) and K14-fluoresence stained skin sections. Scale bars, 50 μm. **c**, Peyer's patches are present in the small intestine of wild-type (WT) but not of *cpdm* or *cpdm*;*Tnf*$^{-/-}$ mice as shown by 'Swiss roll' preparations. Scale bars, 2.5 mm (left panels), 500 μm (right panels). **d**, Spleen architecture of *cpdm* mice is not rescued by additional TNF ablation. Red, CD3; green, B220; blue, nuclei. Scale bars, (from left to right) 500 μm, 200 μm, 50 μm and 50 μm. **e**, SHARPIN-deficient primary keratinocytes are sensitive to TNF-induced cell death. Wild type $n = 6$, *cpdm*;*Tnf*$^{-/-}$ $n = 2$, *cpdm*;*Tnf*$^{-/+}$ $n = 4$, except TNF+NEC, TNF+QVD and TNF+NEC+QVD, where $n = 3$.

aspects of the immunological phenotype of *cpdm* mice were unaltered in *cpdm*;*Tnf*$^{+/-}$ and *cpdm*;*Tnf*$^{-/-}$ mice; Peyer's patches remained absent (Fig. 5c and Supplementary Fig. 22a), spleens remained without marginal zones (Fig. 5d) and enlarged, albeit, on average, to a somewhat lesser degree than the *cpdm* spleens (Supplementary Fig. 22b). In addition, the blood cell counts of various leukocyte populations also remained abnormal in TNF-deficient *cpdm* mice (Supplementary Fig. 22c). Hence, the inflammatory phenotype of *cpdm* mice is corrected by genetic ablation of TNF, identifying it as TNF-dependent, whereas the immunological phenotype of *cpdm* mice remains unaltered by TNF deficiency.

Given that skin inflammation is so pivotal in the inflammatory manifestation of the *cpdm* phenotype, we examined the skin phenotype of *cpdm;Tnf*$^{-/-}$ mice in more detail. Histological examination of the skin revealed that, as previously reported[13], *cpdm* mice have hyperkeratosis with some parakeratosis (Fig. 5b). In *cpdm*;*Tnf*$^{+/-}$ (Supplementary Fig. 21), and particularly in *cpdm*;*Tnf*$^{-/-}$ mice, this was almost completely absent (Fig. 5b). Likewise, the immune cell infiltrate, readily apparent in sections from livers of *cpdm* mice and present as nodular lymphocyte aggregates distributed around the central vein branches, was absent in *cpdm*;*Tnf*$^{+/-}$ (not shown) and *cpdm*;*Tnf*$^{-/-}$ mice (Fig. 5b). Combined with our observations that *cpdm* MEFs were more susceptible to TNF-induced cell death and that genetic ablation of TNF corrected the inflammatory phenotype in *cpdm* mice, including the inflammatory skin disease, we reasoned that one potential explanation for the inflammatory phenotype could be increased sensitivity of *cpdm* keratinocytes to TNF-induced cell death. This hypothesis was further supported by our finding that TNF-induced NF-κB and JNK activation were reduced in *cpdm*-derived keratinocytes (Supplementary Fig. 18) and by a report describing increased rates of keratinocyte cell death observed in the skin of *cpdm* mice[14]. We found that primary keratinocytes derived from lesion-free *cpdm*;*Tnf*$^{-/-}$ and *cpdm*;*Tnf*$^{+/-}$ mice were sensitive to TNF-induced cell death, whereas keratinocytes derived from wild-type mice were not (Fig. 5e). As for *cpdm* MEFs, the cell death induced by TNF in SHARPIN-deficient keratinocytes was partially apoptotic and partially necroptotic. This result immediately suggests an explanation for the initiation and subsequent worsening of the skin phenotype, namely that *cpdm* keratinocytes are prone to die when exposed to TNF in the skin, some of them by necroptosis, some of them by apoptosis which may also lead to secondary necrosis. Because necroptosis and secondary necrosis are pro-inflammatory forms of cell death they initiate the vicious circle of inflammation and the inflammatory phenotype progressively worsens over time.

Discussion

We show that SHARPIN is recruited to native TNF- and CD40-RSCs, forms part of the tripartite LUBAC and is required for this complex's stability. SHARPIN also has a physiological role in lymphoid system development and suppression of inflammation. The genetic ablation of TNF completely resolved skin lesions in *cpdm* mice, demonstrating that the inability of *cpdm* cells to signal properly in response to TNF results in inflammation. It was recently shown that genetic ablation of the IL-1 receptor accessory protein (IL-1RAcP) reduced, but did not prevent, skin inflammation in these mice[19]. Our data show that, like TNF signalling, IL-1β-induced NF-κB and JNK activation is also impaired in *cpdm*-derived keratinocytes. One model that integrates both findings would be that dying *cpdm* keratinocytes stimulate increased production of IL-1β or related cytokines that require the IL-1RAcP for signalling[20,21]. These cytokines could contribute to inflammatory lesions in *cpdm* mice directly or by promoting the production of additional pro-inflammatory cytokines. This highly inflammatory milieu, caused by TNF-induced cell death, promotes inflammation despite the observed reduction in the absolute signalling capacity of IL-1β in *cpdm*-derived primary keratinocytes. However, more work will be required to dissect and fully comprehend the disease process.

K48- and K63-linked ubiquitin chains and their physiological roles in protein degradation or intracellular signalling, respectively, are well established[4]. However, recent data claimed active roles also for other ubiquitin chain linkages, particularly for M1-linked chains on NEMO[5,6,22–24]. We now demonstrate the presence of M1-linked ubiquitin chains on RIP1 and NEMO in the native TNF-RSC. *In vitro* LUBAC can add linear ubiquitin chains to NEMO, but only very inefficiently to RIP1. LUBAC may therefore preferentially linearly ubiquitinate pre-existing ubiquitin moieties on RIP1 or, alternatively, RIP1 only serves as a LUBAC substrate in a properly composed TNF-RSC. It is possible that other proteins, in addition to RIP1 and NEMO, could be targeted by LUBAC in this and other signalling complexes. The determination of the exact ubiquitination pattern and timing of these modifications on individual components of signalling complexes will be required to understand better how signalling from receptor-associated and intracellular signalling complexes is controlled[25,26]. We believe that the application of the moTAP-2D-MRM technique is likely to contribute to this endeavour.

Our findings point towards a complex network of interactions between proteins modified by ubiquitin and proteins recruited to specific ubiquitin linkages. Presence of certain linkage types, such as linear ubiquitin chains, may promote recruitment of factors such as NEMO. However, absence of a linkage like linear ubiquitin does not imply that recruitment of these factors will not occur. For example, NEMO binds to M1-linked but can also bind to K63-linked chains, albeit with lower affinity[7] or different topology[27]. Additionally, NEMO has been shown recently to bind to K11-linked chains[28] which, incidentally, we identified on TNF-RSC-recruited RIP1. Adjusting levels of particular ubiquitin chains does, however, suggest a mechanism by which signal strength can be adjusted and, as demonstrated here for SHARPIN mutants, may lead to significant alterations in physiological outcome. Thus, the regulated expression of factors that generate a particular linkage type, for example, of LUBAC components, may enable a versatile fine-tuning of signalling output with respect to the differentiation stage and/or cell type, and dysregulation of such a factor may lead to a patho-physiological outcome. We therefore predict that germ-line mutations in human genes encoding LUBAC components will cause auto-inflammatory manifestations reminiscent of the *cpdm* phenotype. Patients with auto-inflammatory disease with unknown aetiology should therefore be screened for such mutations and, if found, our data further suggest that inhibition of TNF may alleviate many of their symptoms.

Along the same line of thought, our results also provide a possible alternative explanation for the aetiology of autoimmune diseases and the therapeutic effect of TNF inhibitors in treating them, even in cases when other, non-specific anti-inflammatory drugs fail[29]. The current concept is that TNF inhibitors work in rheumatoid arthritis, Crohn's disease, psoriasis and other auto-immune diseases by interfering with the gene-inducing arm of TNF signalling, that is, the part of the pathway which is so far thought to be the source of pro-inflammatory signals induced by this cytokine[30]. Based on our data an alternative explanation could be, however, that dysregulated expression or somatic mutation of a TNF signalling pathway component, for example, of one of the LUBAC components or a cIAP, would unbalance TNF signalling output in favour of pro-inflammatory cell death. This would then cause TNF to induce inflammation and, consequently, autoimmunity. If this were the case, TNF inhibition would exert its therapeutic effect by inhibiting TNF-induced pro-inflammatory cell death as the disease-initiating principle. It will be interesting to test this provocative hypothesis experimentally, both for our understanding of the basic mechanisms of immune signalling and in our quest for new therapeutic options in autoimmunity and possibly also in inflammation-associated cancer[31–33].

METHODS SUMMARY

Fluorescence-labelling of moTAP-purified TNF-RSC components, two-dimensional electrophoresis and MRM mass spectrometry. The moTAP-purified

TNF-RSC was eluted in two sequential steps, each performed with 2D lysis buffer. Eluted proteins were minimally fluorescently labelled by incubation with Cydyes 2, 3 or 5 (GE Healthcare). Labelling was stopped by addition of L-lysine. Labelled proteins were adjusted to 20 mM DTT and 1% IPG buffer, before cup loading onto either pH 3–11 NL or pH 4–7 rehydrated Immobiline Drystrips (GE Healthcare), and separated on an Ettan IPGphor II (GE Healthcare). After IEF, the Immobiline strip was washed with equilibration buffer (65 mM DTT) and then equilibration buffer (135 mM iodoacetamide) before second dimension electrophoresis (Bio-Rad Criterion). Fluorescence images of the resulting 2D gels (Typhoon Trio, GE Healthcare) were used to guide robotic spot picking (Ettan spot picker, GE Healthcare). Proteins contained in picked spots were digested with trypsin and analysed using MRM with a 4000 QTRAP mass spectrometer. In the first part of this MS analysis, the instrument was used as a triple quadrupole mass spectrometer to perform MRM analyses to screen for specific proteins and ubiquitin (including linkage-specific tryptic peptides that contain the Gly-Gly motif bound to the ε-amino group of lysine residues, or N-terminal Gly-Gly for the M1 linear peptide). The second phase of the analysis uses the third quadrupole as a linear ion trap for product ion detection to confirm peptide identification.

Full Methods and any associated references are available in the online version of the paper at www.nature.com/nature.

Received 8 April 2010; accepted 11 January 2011.

1. Ware, C. F. The TNF superfamily. *Cytokine Growth Factor Rev.* **14,** 181–184 (2003).
2. Bianchi, K. & Meier, P. A tangled web of ubiquitin chains: breaking news in TNF-R1 signaling. *Mol. Cell* **36,** 736–742 (2009).
3. Silke, J. & Brink, R. Regulation of TNFRSF and innate immune signalling complexes by TRAFs and cIAPs. *Cell Death Differ.* **17,** 35–45 (2010).
4. Wertz, I. E. & Dixit, V. M. Ubiquitin-mediated regulation of TNFR1 signaling. *Cytokine Growth Factor Rev.* **19,** 313–324 (2008).
5. Haas, T. L. *et al.* Recruitment of the linear ubiquitin chain assembly complex stabilizes the TNF-R1 signaling complex and is required for TNF-mediated gene induction. *Mol. Cell* **36,** 831–844 (2009).
6. Tokunaga, F. *et al.* Involvement of linear polyubiquitylation of NEMO in NF-κB activation. *Nature Cell Biol.* **11,** 123–132 (2009).
7. Rahighi, S. *et al.* Specific recognition of linear ubiquitin chains by NEMO is important for NF-κB activation. *Cell* **136,** 1098–1109 (2009).
8. Lo, Y. C. *et al.* Structural basis for recognition of diubiquitins by NEMO. *Mol. Cell* **33,** 602–615 (2009).
9. Komander, D. *et al.* Molecular discrimination of structurally equivalent Lys 63-linked and linear polyubiquitin chains. *EMBO Rep.* **10,** 466–473 (2009).
10. Xu, M., Skaug, B., Zeng, W. & Chen, Z. J. A ubiquitin replacement strategy in human cells reveals distinct mechanisms of IKK activation by TNFα and IL-1β. *Mol. Cell* **36,** 302–314 (2009).
11. Cossu, F. *et al.* Structural basis for bivalent Smac-mimetics recognition in the IAP protein family. *J. Mol. Biol.* **392,** 630–644 (2009).
12. Seymour, R. E. *et al.* Spontaneous mutations in the mouse *Sharpin* gene result in multiorgan inflammation, immune system dysregulation and dermatitis. *Genes Immun.* **8,** 416–421 (2007).
13. HogenEsch, H. *et al.* A spontaneous mutation characterized by chronic proliferative dermatitis in C57BL mice. *Am. J. Pathol.* **143,** 972–982 (1993).
14. HogenEsch, H., Janke, S., Boggess, D. & Sundberg, J. P. Absence of Peyer's patches and abnormal lymphoid architecture in chronic proliferative dermatitis (*cpdm/cpdm*) mice. *J. Immunol.* **162,** 3890–3896 (1999).
15. HogenEsch, H. *et al.* Increased expression of type 2 cytokines in chronic proliferative dermatitis (*cpdm*) mutant mice and resolution of inflammation following treatment with IL-12. *Eur. J. Immunol.* **31,** 734–742 (2001).
16. Tay, S. *et al.* Single-cell NF-κB dynamics reveal digital activation and analogue information processing. *Nature* **466,** 267–271 (2010).
17. Senftleben, U. *et al.* Activation by IKKα of a second, evolutionary conserved, NF-κB signaling pathway. *Science* **293,** 1495–1499 (2001).
18. Gijbels, M. J., HogenEsch, H., Bruijnzeel, P. L., Elliott, G. R. & Zurcher, C. Maintenance of donor phenotype after full-thickness skin transplantation from mice with chronic proliferative dermatitis (*cpdm/cpdm*) to C57BL/Ka and nude mice and vice versa. *J. Invest. Dermatol.* **105,** 769–773 (1995).
19. Liang, Y., Seymour, R. E. & Sundberg, J. P. Inhibition of NF-κB signaling retards eosinophilic dermatitis in SHARPIN-deficient mice. *J. Invest. Dermatol.* **131,** 141–149 (2011).
20. Martin, M. U. & Wesche, H. Summary and comparison of the signaling mechanisms of the Toll/interleukin-1 receptor family. *Biochim. Biophys. Acta* **1592,** 265–280 (2002).
21. Arend, W. P., Palmer, G. & Gabay, C. IL-1, IL-18, and IL-33 families of cytokines. *Immunol. Rev.* **223,** 20–38 (2008).
22. Huang, H. *et al.* K33-linked polyubiquitination of T cell receptor-ζ regulates proteolysis-independent T cell signaling. *Immunity* **33,** 60–70 (2010).
23. Matsumoto, M. L. *et al.* K11-linked polyubiquitination in cell cycle control revealed by a K11 linkage-specific antibody. *Mol. Cell* **39,** 477–484 (2010).
24. Arimoto, K. *et al.* Polyubiquitin conjugation to NEMO by triparite motif protein 23 (TRIM23) is critical in antiviral defense. *Proc. Natl Acad. Sci. USA* **107,** 15856–15861 (2010).
25. Ikeda, F., Crosetto, N. & Dikic, I. What determines the specificity and outcomes of ubiquitin signaling? *Cell* **143,** 677–681 (2010).
26. Liu, S. & Chen, Z. J. Expanding role of ubiquitination in NF-κB signaling. *Cell Res.* **21,** 6–21 (2011).
27. Laplantine, E. *et al.* NEMO specifically recognizes K63-linked poly-ubiquitin chains through a new bipartite ubiquitin-binding domain. *EMBO J.* **28,** 2885–2895 (2009).
28. Dynek, J. N. *et al.* c-IAP1 and UbcH5 promote K11-linked polyubiquitination of RIP1 in TNF signalling. *EMBO J.* **29,** 4198–4209 (2010).
29. Taylor, P. C. & Feldmann, M. Anti-TNF biologic agents: still the therapy of choice for rheumatoid arthritis. *Nature Rev. Rheumatol.* **5,** 578–582 (2009).
30. Sacre, S. M., Andreakos, E., Taylor, P., Feldmann, M. & Foxwell, B. M. Molecular therapeutic targets in rheumatoid arthritis. *Expert Rev. Mol. Med.* **7,** 1–20 (2005).
31. Mantovani, A., Allavena, P., Sica, A. & Balkwill, F. Cancer-related inflammation. *Nature* **454,** 436–444 (2008).
32. Pikarsky, E. *et al.* NF-κB functions as a tumour promoter in inflammation-associated cancer. *Nature* **431,** 461–466 (2004).
33. Grivennikov, S. I., Greten, F. R. & Karin, M. Immunity, inflammation, and cancer. *Cell* **140,** 883–899 (2010).

Supplementary Information is linked to the online version of the paper at www.nature.com/nature.

Acknowledgements We thank M. Miasari for developing the cIAP2 antibody, M. Leverkus for advice on skin histology, J. Lokan for advice on liver histology, C. Rappl, N. Barboza, S. Kupka, D. Heinze, J. Zipprich, J. Corbin, S. Wiegelmann and A. Bankovacki for excellent technical assistance, M. Bolognesi and P. Seneci for SM-164, H. Koerner for *Tnf*$^{-/-}$ *mice, and all past and present members of the Walczak and Silke laboratories for continuous stimulating scientific discussions and support. Research in the Walczak lab is supported by grants from Cancer Research UK, AICR, BBSRC (ERASysBio PLUS), Ovarian Cancer Action and the EU Marie Curie Research Training Network ApopTRAIN. Work in the Silke lab is supported by NHMRC grants 541901, 541902 and 602516. Work in the Purcell lab is supported by the NHMRC (Senior Research Fellowships for A.W.P. and a C. J. Martin Overseas Biomedical Fellowship to A.I.W.), and by grants from the NHMRC and ARC. U.W. is funded by HGF/SBCancer. E.R. and T.L.H. are ApopTRAIN fellows and U.N. is supported by the Schweizer Nationalfonds (SNF).*

Author Contributions T.L.H. and H.W. conceived the moTAP procedure. B.G., E.R., H.W. and U.W., and T.L.H. and U.W. determined the composition of the CD40- and TNF-RSC, respectively. B.G. performed all other experiments involving CD40L. A.C.S. and C.H.E. cloned and purified all recombinant proteins, determined the molecular interaction between the LUBAC components and performed the *in vitro* ubiquitination assays. B.G., S.M.C., A.C.S., C.H.E. and E.R. provided moTAP-purified TNF-RSCs for 2D-MRM analysis which was conceived by A.I.W. and H.W., performed by A.I.W., and analysed by A.I.W. and A.W.P.; J.S. and H.W. planned and J.A.R., H.A., U.N., W.W.-L.W., L.G., B.G., S.M.C. and E.R. performed the analyses of cells, tissues and blood samples obtained from all mouse strains used in this study. H.W. and J.S. wrote the manuscript assisted by B.G., S.M.C., A.C.S., C.H.E., E.R. and A.I.W.

Author Information Reprints and permissions information is available at www.nature.com/reprints. The authors declare competing financial interests: details accompany the full-text HTML version of the paper at www.nature.com/nature. Readers are welcome to comment on the online version of this article at www.nature.com/nature. Correspondence and requests for materials should be addressed to H.W. (h.walczak@imperial.ac.uk).

METHODS

Reagents. Antibodies used were: anti-CD40 (H-120), anti-IκBα (C-15), anti-p65 (A), anti-TNFR1 (H-5), anti-TRADD (H-278), anti-TRAF2 (C-20), anti-TRAF3 (H122), anti-TRAF6 (D10) and anti-V5 (sv5-pk) from Santa Cruz Biotechnology; anti-Ub (FK1 and FK2) and anti-PARP (C-2-10) from Biomol; anti-Ub (#07-375) from Millipore; anti-Bid (#2002), anti-JNK (56G8), anti-NIK (4994), anti-p100 (4882), anti-pIκBα (5A5) and anti-pJNK (98F2) from Cell Signaling; anti-myc (9E10) and anti-TNFR1 (ab19139) from Abcam; anti-cIAP Pan (MAB3400) from R&D Systems; anti-Caspase 8 (ALX-804-429) from Axxora life sciences; anti-RIP1 (#610459), anti-TRADD (clone37) and anti-mouse FITC-conjugated (554334) from BD Biosciences; anti-GST from Amersham, anti-HA (3F10) and anti-His (BMG-His-1) from Roche Applied Science; anti-A20 (59A426) from Imgenex and anti-Actin (A5441), anti-Flag (M2) from Sigma. Anti-cIAP1 monoclonal antibodies and anti-cIAP2 mAbs were generated as described[34]. Anti-HOIL-1 and anti-HOIP antibodies were previously described[5]. SM-164 (Smac059) was synthesized and provided by P. Seneci and L. Manzoni[11]. Murine B cells were isolated from the spleen with CD43 (Ly-48) MicroBeads according to the manufacturer's protocol (Miltenyi Biotec). Primary murine keratinocytes were stimulated with recombinant IL-1β from Enzo Life Sciences.

Generation of SHARPIN antibody. A monoclonal antibody specific for SHARPIN was generated from 8-week-old Balb/c × C57BL/6 mice which were immunised with KLH-coupled peptide (GPDAEAQLRRLQLSADC).

Cell lines. Wild-type and *cpdm* MEFs were generated from E15 embryos in accordance with standard procedures and were infected with SV40 large T antigen-expressing lentivirus. HEK293-NF-κB cells were purchased from Panomics.

Mice. *Tnf*$^{-/-}$ mice[35] were a gift from H. Körner and *cpdm* mice were obtained from The Jackson Laboratory. Colonies were kept under conventional conditions. *Cpdm* mice were crossed with *Tnf*$^{-/-}$ mice and typed by PCR and sequencing.

Expression and purification of recombinant proteins. The extracellular portion of CD40L was cloned into the pCDNA3.1 expression vector (Invitrogen) in which a new N-terminal moTAP tag, consisting of a double Flag epitope, a PreScission cleavage site (LEVLFQ/GP) and a human Fc-portion, was integrated. Recombinant moTAP-CD40L was expressed in HEK293T cells and collected 24 and 48 h after transfection.

His-Flag-TNF (HF-TNF)[36] and moTAP-TNF[5] were generated as described. Unless stated otherwise, the TNF used in this study was HF-TNF.

HOIP-V5/His and its mutants (HOIP ΔC terminus (residues 1–654), ΔUBA (deletion of residues 564–615), ΔN terminus (residues 494–end)] were previously described[5]. Untagged or V5/His-tagged versions of SHARPIN were generated by PCR and cloned into pcDNA3.1 (Invitrogen). The following mutants were used: SHARPIN ΔUBL (deletion of residues 219–289), SHARPIN ΔNZF (deletion of residues 348–377), SHARPIN NZFmut1 (point mutations of cysteines 353 and 356 to serine) and SHARPIN NZFmut2 (point mutations of cysteines 367 and 370 to serine). The specific point-mutants were obtained by site-directed mutagenesis. All mutations and deletions were verified by sequencing.

Recombinant SHARPIN, HOIL-1, HOIP, SHARPIN-UBL-only (residues 218–314), HOIP-ZnF-only (residues 298–329), HOIP-NZF1-only (residues 350–379), HOIP-NZF2-only (residues 408–438) and TRAF6 were expressed from a pGEX-6P2-vector (GE Healthcare Life Sciences) in *Escherichia coli* BL21(DE3) pLysS (Invitrogen) after addition of 1 μM IPTG and 200 μM $ZnSO_4$ at 18 °C overnight. The proteins were purified with GSTrap FF columns according to the manufacturer's protocol (GE Healthcare Life Sciences). The GST-tag was removed by incubation with PreScission protease (GE Healthcare Life Sciences) and quality was controlled by SDS–PAGE and Coomassie staining.

Western blotting. Western blot analyses were performed as previously described[5]. The quantification of western blots was done with ImageJ software. Briefly, the background was subtracted of the 8-bit greyscale image with a rolling ball radius of 50. The image was inverted and the rectangular selection tool used to frame the band tight on each side. Every lane was selected and analysed. The remaining background was cut off with the straight line selection tool and the area selected with the magic wand. Each p100 band was standardised to its respective actin control levels.

Precipitation of the TNF-RSC. Analytical and preparative precipitation of the TNF-RSC as shown in Fig. 1b was performed as described previously[5].

Tandem affinity purification of the CD40-RSC. Raji cells (3.5×10^9) were stimulated with 50 ml moTAP-CD40L-containing supernatant (approximately 50 μg ml^{-1}) at 37 °C for 10 min. Cells were washed twice with ice-cold PBS and lysed in 1.2 ml IP-lysis buffer/10^8 cells with 0.5% NP-40 at 4 °C for 30 min. The detergent-insoluble fraction was pelleted (30 min; 15,000*g*) and the cell lysate was incubated with 4 μl M2 beads per 10^8 cells (Sigma) for 8 h. Beads were washed four times with 1 ml IP-lysis buffer and subsequently incubated in 1 ml lysis buffer containing 5 U ml^{-1} PreScission (GE Healthcare Life Sciences) and 250 μg ml^{-1} Flag-peptide (Sigma) for 12 h. Protein complexes were eluted from the beads, and the beads were rinsed once with 500 μl IP-lysis buffer. The second precipitation step was carried out using 25 μl Protein G-coupled beads (GE Healthcare Life Sciences) at 4 °C for 6 h. The beads were washed four times and proteins were directly eluted with 3× LDS buffer. The purified CD40-RSC was loaded on a NuPAGE gel. The gel was silver-stained using a mass-spectrometry compatible protocol (Invitrogen) and photo-documented before the lane containing the CD40-RSC was cut into 24 pieces of equal size. The gel pieces were then destained according to the manufacturer's protocol, subjected to tryptic digest as previously described[5] and used for mass spectrometric analysis.

Liquid chromatography tandem mass spectroscopy (LC-MS/MS). The peptide mixtures from the purified receptor complexes in Supplementary Fig. 2 were separated on-line with a split free nano AQUITY UPLC (Waters) using a Symmetry 5 μm C_{18} 20 × 0.18 mm precolumn and a 1.7 μm BEH130 C_{18} 100 × 0.1 mm column (Waters) at a flow rate of 400 nl min^{-1} using a 60 min 5–90% acetonitrile/water gradient. Both gradient solvents were spiked with 0.1% formic acid. The electrospray voltage was set to 2.4 kV. Peptides were analysed using a linear trap/Orbitrap (LTQ-Orbitrap) hybrid mass spectrometer (Thermo Electron). Peptide precursor ion scans were acquired with the Orbitrap mass analyser, the resolving power was set at 60,000 ($m/\Delta m_{50\%}$ at m/z 400). Simultaneously, six MS/MS spectra of the most abundant peptide precursor ions were acquired in the LTQ. Dynamic exclusion was used with two repeat counts, 20 s repeat duration, and 30 s exclusion duration. Mass-spectrometric analysis of the TNF-RSC as shown in Fig. 1b was performed as described previously[5].

Protein identification. Processed data were searched against the National Center for Biotechnology Information (NCBI) non-redundant database (2010-02-03; 1,0395,027 sequences total) using the Mascot algorithm version v2.2.0 (Matrix Science). The algorithm was set to use *Homo sapiens* as taxonomy (229,496 protein sequences). The following search parameters were selected: fixed carbamidomethyl modification on cysteine side chain, variable modification due to methionine oxidation, deamidation to asparagine and glutamine, glycine dipeptide modification on lysine, one missed cleavage site in the case of incomplete trypsin hydrolysis. The mass tolerance was set to 5 p.p.m. for precursor ions and 0.6 Da for fragment ions. A fragment ions score cut-off of 20 was applied when performing the search. Protein hits were taken as identified if the individual scoring value of at least one peptide match exceeded the Mascot identity threshold (typically a score of ≥ 36; $P \leq 0.05$). Repeated matches of the same peptide in different forms (charge state or modifications) were combined into one single hit.

Generation of MRM transitions. The acquisition method consisted of an enhanced MS scan (EMS) with a scan rate of 1,000 Da s^{-1} and four enhanced product ion (EPI) scans with 4,000 Da s^{-1} scan rate. Each of EPI scans had a linear ion trap fill time of 80 ms with unit Q1 resolution, and either doubly or triply charged masses of each peptide were selected as the target masses. The mass range for EMS analysis was 400 to 1,000 Da and 60 to 1,000 Da for the EPI scans. To determine the best collision energy (CE) to use to achieve the optimum multiple reaction monitoring (MRM) transitions for each of the peptides, the collision energy (CE) for the scans were ramped from 16 to 40 eV with an increment of 4 eV. The three highest intensity fragment ions from the MS/MS spectrum obtained with the optimum CE for each peptide were selected as the Q3 mass for the MRM scanning method: All MRM transitions were combined into a single acquisition method for sample analysis. Refer to Supplementary Fig. 10 for a list of all peptide MRM transitions.

CyDye labelling and 2D gel electrophoresis. TNF-RSC was eluted from Protein G beads with 100 μl of 2D lysis buffer, which contains 7 M urea, 2 M thiourea, 4% CHAPS and 40 mM Tris buffered to pH 8.5 at 4 °C. Cydyes 2, 3 or 5 (100 pmol each, GE Healthcare) were used to minimally label eluted proteins for 30 min on ice. L-lysine (1 μl of 10 mM) was then added for a further 10 min. Labelled proteins were adjusted to 20 mM DTT and 1% IPG buffer, before being loaded by cup loading onto either pH 3–10 or pH 4–7 rehydrated 11 cm Immobiline Drystrip (GE Healthcare) and run using manufacturer's recommended settings. The Immobiline strip was then washed with equilibration buffer (GE Healthcare) containing 65 mM DTT and 135 mM Iodoacetamide for 15 min each. Equilibrated gel strips were then loaded and run on 8–16% gradient Criterion Tris-HCl gel (Bio-Rad). 2D gels were then imaged on a Typhoon Trio (GE Healthcare) using default settings for CyDyes. Protein-containing spots were identified and selected using ImageMaster 2D Platinum v7.0 software (GE Healthcare) and were robotically excised by an Ettan Spot Picker (GE Healthcare). Gel pieces were washed using 100 mM TEAB (triethylammonium bicarbonate, pH 8.5) in 50% (v/v) acetonitrile. Gel pieces were dehydrated using 100% (v/v) acetonitrile and air-dried. Dried gel pieces were rehydrated in the presence of 250 ng sequencing grade trypsin (Sigma) in 50 mM TEAB. Digests were allowed to proceed overnight at 37 °C.

MRM mass spectrometry. Chromatographic separation of peptides picked from 2D gels (Fig. 3) was performed before MS analysis using a Shimadzu Prominence UFLC coupled with a pre-packed 300 μm internal diameter × 10 mm ReproSil

C18-AQ 5 μm trap column (SGE) and a 15 μm tip internal diameter, 75 μm capillary internal diameter, 360 μm OD fused-silica PicoFrit nano analytical column (New objective) packed with 15 cm of ReproSil-Pur C18-AQ 5 μm resin (Dr. Maisch). Gel digests were loaded onto the trap column using the auto-sampler with a flow rate of 100 μl min^{-1} 0.1% formic acid and separated using a step gradient with mobile phase A consisting of 0.1% formic acid and mobile phase B consisting of 95% acetonitrile and 0.1% formic acid. Peptides eluting off the reverse-phased column were analysed using a 4000 Q TRAP hybrid triple quadrupole-linear ion trap-mass spectrometer (AB SCIEX) in positive ion mode. The acquisition method was set to perform a MRM scanning experiment and an information-dependent acquisition (IDA) of a full mass MS/MS spectrum in EPI mode triggered by MRM transitions that exceeded 200 counts. An AB SCIEX nanospray II ion source was used for ionisation with the ion spray voltage (IS) set at 2,200 V, curtain gas (CUR) at 22, ion source gas (GS1) at 25, high collision gas (CAD), and an interface heater temperature setting of 90. For the SRM transitions, the dwell time for each transition was fixed at 40 ms with the resolution of the first (Q1) and third (Q3) quadrupole operating at unit resolution. A scan rate of 1000 Da s^{-1} was used for the EPI scan with a scanning m/z range of 70 to 1,500 Da, a fixed LIT fill time of 80 ms, and the Q1 resolution set to unit.

Gel filtration. HeLa cells were lysed in lysis buffer containing 50 mM Tris–HCl, pH 7.5, 1 mM $MgCl_2$, 1 mM DTT and a protease inhibitor cocktail (Complete EDTA-free, Roche) by repeated passing through a syringe needle. After adding an equal volume of lysis buffer containing 300 mM NaCl, lysates were centrifuged at 100,000*g* for 60 min to obtain S100 lysates. S100 lysates were separated via a Superdex 200 10/300 GL column (GE Healthcare Life Sciences) in 50 mM Tris–HCl pH 7.5, 150 mM NaCl using an ÄKTA chromatography system (GE Healthcare Life Sciences).

NF-κB luciferase assay. HEK293-NF-κB cells were transfected with plasmids encoding the indicated proteins using Fugene6 (Roche Applied Science). Cells were lysed in passive lysis buffer (Promega Corporation) 16 h post transfection and luminescence was measured using a microplate reader (Mithras LB940; Berthold Technologies). Viability was controlled by MTT (3-[4,5-dimethyl thiazol-2-yl-2,5-diphenyltetrazolium] bromide) measurement.

***In vitro* transcription/translation.** For *in vitro* binding assays, SHARPIN, HOIP and their respective mutants were generated *in vitro* using the TNT Quick Coupled Transcription/Translation System (Promega Corporation) according to the manufacturer's instructions. Equal protein production was controlled by western blotting.

***In vitro* ubiquitination assay.** For *in vitro* ubiquitination assays, 0.8 μg recombinant HOIP, HOIL-1 and GST–SHARPIN were incubated with 5 μg ubiquitin, 200 ng E1 (UBE1), 300 ng E2 (UbcH5c), 1 × ERS (Boston Biochem) in ubiquitination buffer (20 mM Tris–HCl pH 7.5, 2 mM DTT, 5 mM $MgCl_2$). After 2 h incubation at 37 °C the reaction was stopped by adding reducing sample buffer (RSB). The samples were analysed by western blotting.

For *in vitro* ubiquitination of potential targets 293T cells were transfected with plasmids encoding a tagged version of the respective protein using calcium phosphate and proteins were immunoprecipitated using beads coupled to antibodies specific for either the tag or the protein itself. The beads were washed, dried and added to the reaction mix. The assay was performed as described above.

Interaction mapping. *In vitro*: 10 μg of recombinant protein were immobilised on Protein G beads using specific antibodies, bound to glutathione beads using their GST-tag or precipitated via their V5-tag using anti-V5-agarose resin (Sigma).The beads were washed three times before *in-vitro*-translated versions of the possible interaction partner, 2 μg of tetra-ubiquitin chains or of the recombinant interaction partner were added, respectively. Co-immunoprecipitation occurred overnight at 4 °C.

In vivo: 7.5×10^6 HEK293T cells were transfected with 5 μg of the respective expression plasmids by standard calcium phosphate transfection. Cells were harvested 24 h post transfection, lysed and immunoprecipitations were performed at 4 °C for 16 h using anti-V5-agarose resin (Sigma). Interactions with ubiquitin were mapped using agarose beads coupled to ubiquitin (Boston Biochem).

Quantitative real-time PCR. RNA purification, cDNA synthesis and quantitative real-time PCR were performed as described previously[5]. The following gene-specific primers were used: 5′-CCCACGCTACCTCTGCTC-3′ and 5′-GATGGATACCTGAGCATCACC-3′ (*ICAM-1*), 5′-ACGAGCAAATGGTGAAGGAG-3′ and 5′-ATGATTGCCAAGTGCAGGA-3′ (*IκBα*), 5′-TGCCTATGTCTCAGCCTCTTC-3′ and 5′-GAGGCCATTTGGGAACTTCT-3′ (*TNF*), 5′-GCTCAACTGGTGTCGTGAAG-3′ and 5′-ATGAGGCAGTTTCCATCACC-3′ (*A20*), 5′-CTGTGCATTTACACCGACAAC-3′ and 5′-CACTACCAGTTCCCACTCCAG-3′ (*CyclinD2*), 5′-CCCAGTGTCACCAGACCTTC-3′ and 5′-CCTCACAACTCCGTCCTCTG-3′ (*HOIP*), 5′-TCTCCCCAACACAGGACATC-3′ and 5′-AAATGGTGACGGTGTGCAT-3′ (*HOIL-1*).

Staining cells for confocal microscopy. Cells were seeded onto cover slips and starved for 6 h before TNF-treatment. After stimulation (50 ng ml^{-1} TNF), cells were washed twice with ice-cold PBS and fixed with 4% paraformaldehyde/PBS for 20 min. Cell membranes were permeabilized with 0.2% Triton in PBS for 5 min. Unspecific binding was blocked with 1% BSA/PBS for 1 h and cells were stained with anti-p65 in a wet chamber at 4 °C overnight. Next, cells were washed three times and incubated with Alexa488-coupled anti-rabbit antibodies (Invitrogen) for 1 h at room temperature. Cells were washed again and nuclei were stained with ProLong Gold antifade reagent containing DAPI (Invitrogen). The p65-positive nuclear area was quantified with the Leica Application Suite software.

Cell death/viability assessment. MEF cells (1×10^5 or 1×10^4) were seeded per 12-well or 96-well, respectively, pre-treated with medium, 10 μM Q-Val-Asp(non-*O*-methylated)-OPh (QVD; R&D Systems) and/or 30 μM necrostatin-1 (NEC; Biomol) before addition of TNF. The percentage of cell death was assessed by propidium iodide (PI) uptake 24 h later. Alternatively, cell viability was measured by Cell Titer Glo (Promega) according to the manufacturer's instructions.

Cytosol/nuclear fractionation. Splenocytes from wild-type and *cpdm* mice (3.5×10^6) were stimulated for different time points with TAP-CD40L-containing supernatant and washed with ice-cold PBS. Cytosolic and nuclear fractions were prepared with NE-Per Nuclear Cytosol Extraction kit (Thermo Fisher Scientific) where the manufacturer protocol was strictly followed.

Histology. For haematoxylin and eosin stain tissues were fixed in 4% paraformaldehyde in PBS. Tissues were embedded in paraffin and sections were stained with haematoxylin and eosin.

For fluorescence stains spleens were frozen in Tissue Tek OCT compound (Sakura). Sections (6 μm) were cut using a CM8500 cryostat (Leica), fixed in acetone and blocked overnight with 3% normal horse serum (SAFC Biosciences). Slides were stained with the following antibodies: anti-CD3e-biotin (eBio500A2, eBiosciences) and anti-B220-FITC (BD Pharmingen). Biotinylated antibodies were detected with streptavidin-Alexa Fluor 555 (Invitrogen). Hoechst (Invitrogen) staining was used to visualize nuclei. Slides were analysed with an Olympus BX-50 fluorescence microscope using ×10 and ×20 objective lenses and the SPOT Advance software. For immunofluorescence stainings of the skin, sections were stained with polyclonal rabbit anti-keratin 14 (Covance) and Alexa-fluor 594 goat-anti-rabbit (Invitrogen). Nuclei were visualized using Hoechst (Invitrogen). Images were acquired using SPOT Advance and processed using ImageJ software.

Keratinocyte culture and cell death assays. Murine tail skin was incubated in keratinocyte serum free media (Invitrogen) supplemented with 50 μg ml^{-1} gentamicin and 2.1 U ml^{-1} dispase II (Roche) at 4 °C overnight. The epidermis was then removed and incubated in TrypLE Express trypsin (Invitrogen) for 10 min with agitation to isolate keratinocytes. Cells were seeded in 24-well plates in keratinocyte media and cultured to at least 70% confluency. Cells were then left untreated or pre-treated with 50 μM Necrostatin-1 (Tetralogics) and/or 10 μM QVD (SM Biochemicals LLC) for 1 h before addition of 100 ng ml^{-1} human Fc-TNFα for a further 24 h. Death was quantified by FACS analysis of PI uptake.

Swiss roll. For Swiss rolls, the intestinal tract from stomach to caecum was harvested and fixed overnight in 4% buffered paraformaldehyde. Intestines were then cut open longitudinally, cleaned from faeces and rolled. The rolls were embedded in paraffin and processed as other tissue slides[37].

34. Silke, J. *et al.* Determination of cell survival by RING-mediated regulation of inhibitor of apoptosis (IAP) protein abundance. *Proc. Natl Acad. Sci. USA* **102,** 16182–16187 (2005).
35. Körner, H. *et al.* Distinct roles for lymphotoxin-α and tumor necrosis factor in organogenesis and spatial organization of lymphoid tissue. *Eur. J. Immunol.* **27,** 2600–2609 (1997).
36. Diessenbacher, P. *et al.* NF-κB inhibition reveals differential mechanisms of TNF *versus* TRAIL-induced apoptosis upstream or at the level of caspase-8 activation independent of cIAP2. *J. Invest. Dermatol.* **128,** 1134–1147 (2008).
37. Moolenbeek, C. & Ruitenberg, E. J. The 'Swiss roll': a simple technique for histological studies of the rodent intestine. *Lab. Anim.* **15,** 57–59 (1981).